25th ABCM International Congress of Mechanical Engineering
October 20-25, 2019, Uberlândia, MG, Brazil

COB-2019-1791
HAMILTONIAN MONTE CARLO METHOD APPLIED IN THE INVERSE ANALYSIS OF FORCED CONVECTION IN MICRO-CHANNELS IN THE SLIP FLOW REGIME

Géssica Ramos da Silva
Maicon de Paiva Torres
Leonardo Tavares Stutz
Diego Campos Knupp
Antônio José da Silva Neto
Polytechnic Institute, Rio de Janeiro State University – IPRJ/UERJ, Nova Friburgo/RJ - Brazil
grsilva@iprj.uerj.br, mptorres@iprj.uerj.br, ltstutz@iprj.uerj.br, diegoknupp@iprj.uerj.br, ajsneto@iprj.uerj.br

Abstract. *In the present work, the direct and inverse analysis of convective heat transfer with incompressible laminar gas flow in micro-channels, within the range of validity of the slip-flow regime, are presented. The direct problem analysis consists in applying the finite difference scheme in the two-dimensional steady-state convection problem. The inverse problem analysis focus on the identification of the momentum and thermal accommodation coefficients, related to gas flow and heat transfer within micro-channels, besides the external Biot number, present in the boundary condition. A comparison between the Metropolis-Hastings algorithm and the Monte Carlo Hamiltonian method is made in the solution of the identification problem for a base case.*

Keywords: *micro-channel, heat transfer, finite difference method*

1. INTRODUCTION

Currently, microchannels are being used in many areas, such as medicine, biotechnology, consumer electronics, computer and safety technology, process engineering, robotics, among others (Rostami *et al.*, 2002). The majority of miniaturized thermomechanical equipments involve the flow of a fluid in microchannels and may also be combined with heat transfer. It is important to notice that there are discrepancies between the flow and heat transfer characteristics of a gas flowing in micro- and macro-scale (Morini, 2004). These discrepancies are mainly related to the fact that scaling effects, such as entrance effects, conjugate heat transfer, viscous heating, electric double layer (EDL) effects, temperature dependent properties, surface roughness, rarefaction and compressibility effects, often negligible in macro-channels, may have a significant influence in microsystems (Rosa *et al.*, 2009).

Among different model modifications proposed to describe more adequately the fluid flow and heat transfer in microchannels, the consideration of slip flow in opposition to the classical no-slip condition, in the case of gaseous microchannel flows, has been the subject of numerous investigations in previous works for different microchannel geometries: circular micro-tubes (Ameel *et al.*, 1997; Larrodé *et al.*, 2000; Hooman and Ejlali, 2010), and rectangular and parallel plates microchannels (Yu and Ameel, 2001; Mikhailov and Cotta, 2005; Cotta *et al.*, 2016).

The accurate simulation of those problems is, however, dependent on an accurate determination of the momentum and thermal accommodation coefficients, required by the slip and temperature jump boundary conditions provided by the slip flow model that accounts for non-continuum effects at the fluid-surface interactions. Some experimental works are available in the literature regarding measurements of the tangential momentum accommodation coefficient (Agrawal and Prabhu, 2008), but few results are available regarding the measurement of the thermal accommodation coefficient (Rader *et al.*, 2005).

In this context, an inverse analysis of forced convection in parallel plates micro-channels within the range of the slip flow regime is performed, as well as in Naveira-Cotta *et al.* (2010). However, in this work the Hamiltonian Monte Carlo method (Neal *et al.*, 2011; Kumar *et al.*, 2017) is adopted for the inverse problem formulation and solution in order to estimate the momentum and thermal accommodation coefficients and the Biot number. We take advantage of prior information generally available regarding the tangential momentum accommodation coefficient and the external Biot number. A comparison against the results obtained through the Metropolis-Hastings algorithm is also presented for a base case (Torres *et al.*, 2018).

2. DIRECT PROBLEM FORMULATION AND SOLUTION METHODOLOGY

Consider the incompressible gas flow in a parallel-plates channel, undergoing forced internal convective heat transfer. The external face of the channel wall exchanges heat with the surrounding environment, at T_∞, different from the inlet gas temperature, with a heat transfer coefficient h. The fluid enters the channel with a fully developed velocity profile, $u(y)$, and with an inlet temperature, T_0. The corresponding Knudsen number is such that falls within the region of validity of the first order slip flow modelling. Figure 1 depicts a schematic representation of this problem.

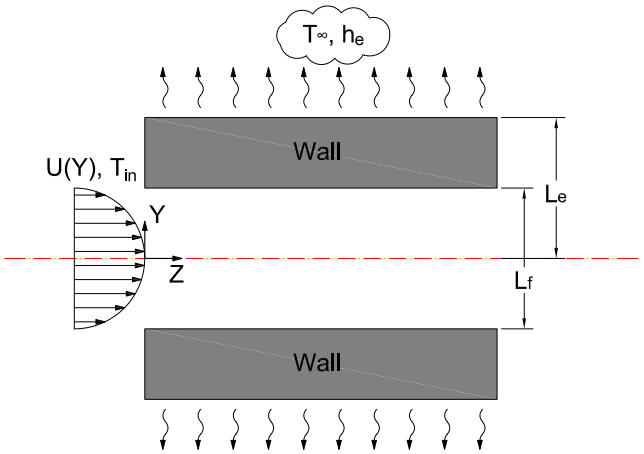

Figure 1. Schematic representation of the convective heat transfer problem with slip flow.

This convective heat transfer problem can then be written as (Naveira-Cotta *et al.*, 2010):

$$W(Y)\frac{\partial \theta^(Y,Z)}{\partial Z} = \frac{\partial^2 \theta(Y,Z)}{\partial Y^2},\ 0<Y<1,\ Z>0 \tag{1a}$$

$$\theta^(Y,0) = 1,\ 0 \le Y \le 1 \tag{1b}$$

$$\left.\frac{\partial \theta}{\partial Y}\right|_{Y=0} = 0,\ \left.\frac{\partial \theta}{\partial Y}\right|_{Y=1} = \frac{Bi}{1+2Kn\beta_t Bi}\theta(1,Z),\ Z>0 \tag{1c,d}$$

where the corresponding dimensionless group are given by

$$\begin{aligned} &Y = \frac{y}{y_1};\ Z = \frac{\alpha z}{u_{a\nu} y_1^2};\ \theta(Y,Z) = \frac{T(y,z)-T_w}{T_0-T_w} \\ &W(Y) = \frac{u(y)}{u_{a\nu}};\ Bi = \frac{h y_1}{k_f};\ Kn = \frac{\lambda}{2y_1} \end{aligned} \tag{2a–f}$$

and,

$$\beta_t = \frac{(2-\alpha_t)}{\alpha_t}\frac{2\gamma}{(\gamma+1)}\frac{1}{Pr} \tag{2g}$$

is the wall temperature jump coefficient and α_t is the thermal accommodation coefficient, λ is the molecular mean free path, $\gamma = \frac{c_p}{c_\nu}$, while c_p is the specific heat at constant pressure, c_ν is the specific heat at constant volume and Pr is the Prandtl number. The dimensionless velocity profile is given as (Mikhailov and Cotta, 2005):

$$W(Y) = \frac{6Kn\beta_v + 3(1-Y^2)/2}{1+6Kn\beta_v} \tag{3a}$$

where,

$$\beta_v = \frac{2-\alpha_m}{\alpha_m} \tag{3b}$$

is the wall velocity slip coefficient and α_m is the tangential momentum accommodation coefficient.

2.1 Finite difference approximation

In this work, the direct problem solution was obtained through finite difference approximation. Therefore, the system of equations (1a–d) was discretized as follows, using an explicit formulation (Anderson *et al.*, 2016):

$$W_{i,j}\frac{\theta_{i,j}-\theta_{i,j-1}}{\Delta Z} = \frac{\theta_{i+1,j}-2\theta_{i,j}+\theta_{i-1,j}}{\Delta Y^2},\ 1 \leq i \leq N_y-1,\ j \geq 1 \tag{4a}$$

$$\theta_{i,1} = 1,\ 0 < i < N_y \tag{4b}$$

$$\frac{\theta_{1,j}-\theta_{-1,j}}{2\Delta Y} = 0,\ 0 \leq j \leq N_z \tag{4c}$$

$$\frac{\theta_{i,j}-\theta_{i-1,j}}{\Delta Y} = \frac{Bi}{1+2Kn\beta_t Bi}\theta_{1,j},\ 0 \leq j \leq N_z \tag{4d}$$

3. INVERSE PROBLEM FORMULATION AND SOLUTION METHODOLOGY

In the Bayesian approach, the inverse problem is formulated as a problem of statistical inference and it is based on the following principles (Kaipio and Somersalo, 2006): (i) the interest parameters of the model are modeled as random variables; (ii) the randomness describes our degree of information; (iii) the degree of information is coded in probability distributions; and (iv) the solution of the inverse problem is the posterior probability distribution. Thus, in the Bayesian approach all possible information is incorporated into the model, aiming to reduce the degree of uncertainty present in the problem.

Consider that some prior information regarding the parameters $\mathbf{P} = [\beta_t, \beta_v, Bi]$ may be available. Assuming that this information can be modeled as a probability density $\pi_{pr}(\mathbf{P})$, Bayes' theorem for inverse problems can be expressed by (Kaipio and Somersalo, 2006):

$$\pi_{post}(\mathbf{P}) = \pi(\mathbf{P}|\mathbf{Y}) = \frac{\pi_{pr}(\mathbf{P})\pi(\mathbf{Y}|\mathbf{P})}{\pi(\mathbf{Y})} \tag{5}$$

where $\pi_{post}(\mathbf{P})$ is the posterior probability density, $\pi_{pr}(\mathbf{P})$ is the prior information of the unknown parameters, $\pi(\mathbf{Y}|\mathbf{P})$ is the likelihood function and $\pi(\mathbf{Y})$ is the marginal density, which acts as a normalization constant. It is important to highlight that the statistical method produces a distribution that can be explored in different ways using different methods.

Consider that the prior information for the parameters can be modeled as a normal distribution. Thus, $\pi_{pr}(\mathbf{P})$ can be expressed by

$$\pi_{pr}(\mathbf{P}) = (2\pi)^{-N_p/2}|\mathbf{V}|^{1/2} exp\left[-\frac{1}{2}(\mathbf{P}-\mu^T)\mathbf{V}^{-1}(\mathbf{P}-\mu)\right] \tag{6}$$

where N_p is the number of parameters, $\mathbf{V}$ and μ are, respectively, the covariance matrix and the mean for $\mathbf{P}$. Replacing Eq. (6) into Eq. (5) and using the likelihood function, one obtains

$$ln[\pi_{post}(\mathbf{P}|\mathbf{Y})] \propto -\frac{1}{2}\left[(N_p+N_d)ln(2\pi) + ln|\mathbf{W}^{-1}| + ln|\mathbf{V}^{-1}| + S_{MAP}(\mathbf{P})\right] \tag{7}$$

where $\mathbf{W}$ is the covariance matrix of the experimental errors, which are supposed to follow a normal distribution, and

$$S_{MAP}(\mathbf{P}) = [\mathbf{Y}-\theta(\mathbf{P})]^T\mathbf{W}^{-1}[\mathbf{Y}-\theta(\mathbf{P})] + [\mu-\mathbf{P}]^T\mathbf{V}^{-1}[\mu-\mathbf{P}] \tag{8}$$

is the objective function of the *maximum a posteriori* (MAP). The minimization of $S_{MAP}(\mathbf{P})$ produces the estimates of $\mathbf{P}$ that maximize the posterior distribution $\pi_{post}(\mathbf{P}|\mathbf{Y})$.

3.1 Markov Chain Monte Carlo Methods

The Markov Chain Monte Carlo method (MCMC) was initially proposed by Metropolis *et al.* (1953), where it was used to simulate states of distribution of idealized molecules. In Bayesian inference, the use of MCMC method aims to calculate the posterior probability density given a set of random variables, when the evaluation of integrals is analytically untreatable. In these cases, the solution of the inverse problem is obtained considering sampling techniques based on the MCMC method. In this work, we use the Metropolis-Hastings (MH) algorithm and the Hamiltonian Monte Carlo method (HMC) in the solution of the inverse problem.

3.1.1 The Metropolis-Hastings Algorithm

One of the simplest Monte Carlo algorithms with Makov chains is the Metropolis-Hastings. In this algorithm, a perturbation of the current position in the parameter space is made by the random selection of a candidate from a symmetric probability distribution. The candidate is accepted or rejected based on the probability of the new position in relation to the previous one.

The first step is to define the starting point in the space vector to be sampled, $\mathbf{Z}^0$. Then, the following algorithm is repeated to obtain the positions $\mathbf{Z}^i$ of the Markov chain's states:

1. Select a new candidate position $\mathbf{Z}^* = \mathbf{Z}^{i-1} + \Delta\mathbf{Z}$, where $\Delta\mathbf{Z}$ is chosen in a random way from an auxiliary distribution $q(\mathbf{Z}^*|\mathbf{Z}^{i-1})$;
2. Calculate the Hastings' ratio, $\alpha = min[1, \pi(\mathbf{Z}^*)/\pi(\mathbf{Z}^{i-1})]$;
3. Generate a random value θ from a uniform distribution in the range $(0, 1)$;
4. Se $\theta < \alpha$, establish $\mathbf{Z}^i = \mathbf{Z}^*$. Otherwise, do $\mathbf{Z}^i = \mathbf{Z}^{i-1}$;
5. Return to the first step to generate the sequence $\{\mathbf{Z}^1, \mathbf{Z}^2, ..., \mathbf{Z}^n\}$.

3.1.2 Hamiltonian Monte Carlo Method

The Hamiltonian Monte Carlo method, or Hybrid Monte Carlo Hybrid method, as is alternatively known, combines the Gibbs sampling with the acceptance function of the Metropolis-Hastings algorithm (Afshar and Sheehan, 2018). The HMC method has a deterministic character inspired by the Hamiltonian dynamics to propose samples following the target probability distribution. Thus, the random walk behavior is attenuated to allow more effective and consistent exploration of the probability space when compared to the Gibbs and Metropolis-Hastings techniques.

The first step in constructing the MCMC method with the Hamiltonian dynamics is to define a Hamiltonian function in terms of the target probability distribution to be sampled. In addition to the variables of interest ("position" variables), it is necessary to introduce "momentum" auxiliary variables, which typically have independent and Gaussian distributions.

In the HMC method, for each parameter Z_i is entered an associated momentum variable, p_i. The Hamiltonian H is then constructed by considering the sum of a potential energy term with a kinetic energy term, in the form

$$H(\mathbf{Z}, \mathbf{p}) = U(\mathbf{Z}) + K(\mathbf{p}) \tag{9}$$

where $U(\mathbf{Z})$ is the negative of the log of the posterior probability distribution, given by $U(\mathbf{Z}) = -log(\pi_{post})$, and $K(\mathbf{p})$ is the kinetic energy, defined by

$$K(\mathbf{p}) = \frac{\mathbf{p}^T \bar{M}^{-1} \mathbf{p}}{2} \tag{10}$$

where $\bar{M}$ is the symmetric and positive-definite mass matrix, which is typically diagonal. This form for $K(\mathbf{p})$ corresponds to the negative of the logarithm of the probability density (plus a constant) of a Gaussian distribution with zero mean and covariance matrix $\bar{M}$.

The partial derivatives of the Hamiltonian determine how $\mathbf{Z}$ and $\mathbf{p}$ change over time t, according to the following equations

$$\frac{dZ_i}{dt} = \frac{\partial H}{\partial p_i}; \ \frac{dp_i}{dt} = -\frac{\partial H}{\partial Z_i}, \ i = 1, 2, ..., N \tag{11a,b}$$

where N is the number of variables (or parameters). For any time interval of duration s, these equations define a mapping, T_s, from the current state, in instant t, to the next state, in instant $t + s$.

Each iteration of the algorithm begins with a Gibbs sampling to generate new momentum variables from the Gaussian distribution, given by kinetic energy. Therefore, the trajectory in the state space $(\mathbf{Z}, \mathbf{p})$ is approximated using the leapfrog integration technique (Anderson *et al.*, 2016), which depends on the number of steps , L, and the step size, ϵ. For $L = 1$ we have the following steps for the integration of the motion equations

$$p_i\left(t + \frac{\epsilon}{2}\right) = p_i(t) - \frac{\epsilon}{2}\frac{\partial U}{\partial Z_i}(\mathbf{Z}(t)) \tag{12a}$$

$$Z_i(t + \epsilon) = Z_i(t) + \epsilon\frac{p_i(t + \frac{\epsilon}{2})}{\bar{m}_i} \tag{12b}$$

$$p_i(t + \epsilon) = p_i(t + \frac{\epsilon}{2}) - \frac{\epsilon}{2}\frac{\partial U}{\partial Z_i}(\mathbf{Z}(t + \epsilon)) \tag{12c}$$

where the gradient of potential energy is obtained, in this work, through finite differences.

4. RESULTS AND DISCUSSION

As real experimental data were not available, they have been simulated in this work by adding a noisy signal, with a controlled level, in the solution of the direct problem in the form:

$$Y_i = T_i(\mathbf{Z_{exact}}) + \sigma e_i,\ i = 1, 2, ..., N_d \tag{13}$$

where $T_i(\mathbf{Z_{exact}})$ corresponds to the calculated values for the temperature using the exact values for the unknown parameters, Z_{exact}, e_i is a random number generated from a normal distribution with zero mean and unit standard deviation, and σ represents the standard deviation of the experimental data. The noise level is calculated by

$$Noise(\%) = max\left|\frac{e_i\sigma}{T_i(\mathbf{Z_{exact}})}\right| * 100\%,\ i = 1, 2, ..., N_d \tag{14}$$

In Figure 2 the temperature distribution over the channel length, Z, for three different transversal positions, $Y = 0.0$, 0.5 and 1.0 is presented. As it can be seen the temperature decays more rapidly in Z than in Y since in this work the axial conduction were not considered in this direction. One can also observe that for $Y = 1.0$ the temperature decays more sharply because of the third type boundary condition (in which there are convection heat transfer), whereas for $Y = 0.0$ there is only prescribed flow.

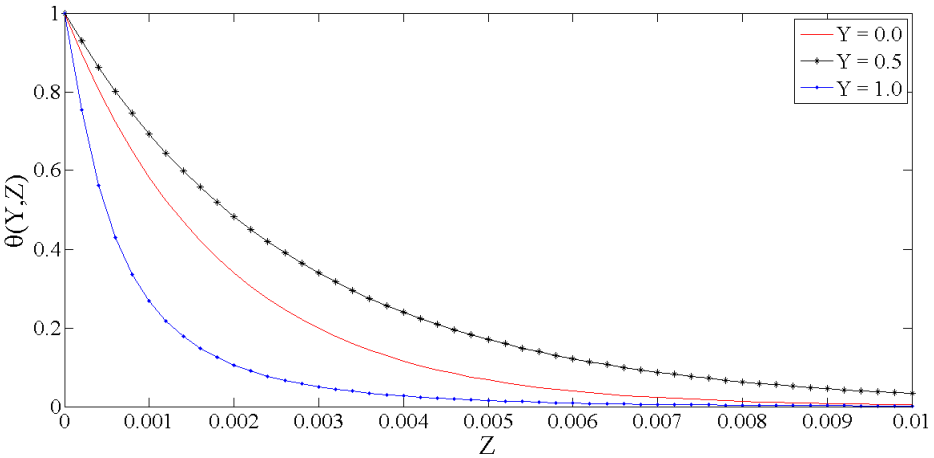

Figure 2. Temperature distribution over the channel length, Z, for different transversal positions.

Now, the inverse problem solution is illustrated. The following typical values of the governing parameters were adopted: β_v = 1.5, β_t = 2.0, Bi = 1.0 and Kn = 0.025. A total of 21 and 51 nodes were used in the Y and Z-direction, respectively, considering Z_f = 0.5.

First of all, we illustrate the Markov chains for each of the three parameters (β_t, β_v and Bi) using the Metropolis-Hastings algorithm (MH) and the Hamiltonian Monte Carlo method (HMC) for a base case with 5% of noise level. The Gaussian priors for the parameters were assumed with means at the exact values and 10% standard deviation. In this case, the chains were started from the average values between the admissible minimum and maximum limits.

Figures 3 (a–c) illustrate the Markov chains (up to 20,000 states) for the estimation of the three parameters, β_t, β_v and Bi, respectively. One may observe the fast Markov chains convergence for both MCMC methods. Up to 1,000 states were enough to achieve the chains steady distributions. The wall temperature jump coefficient, β_t, appears to be the most difficult one to estimate in the present situation. Table 1 brings a summary of the input data and illustrates not only the estimated values, after neglecting the first 2,000 states in each chain, but also the minimum and maximum values of the 95% credibility intervals for the estimated parameters. In all estimations the exact values lies within the credibility intervals.

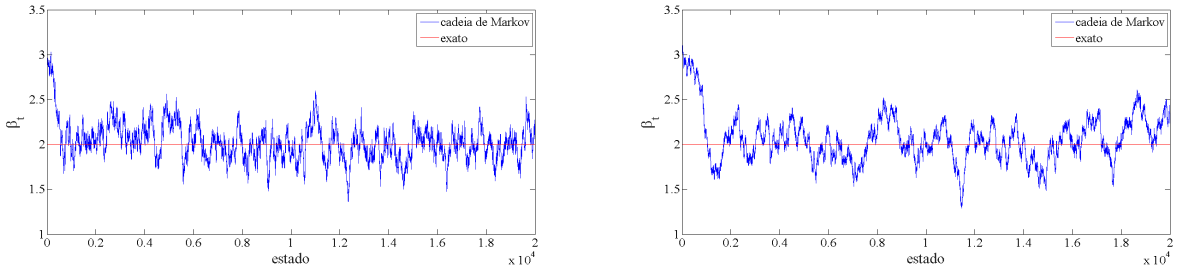

(a) β_t

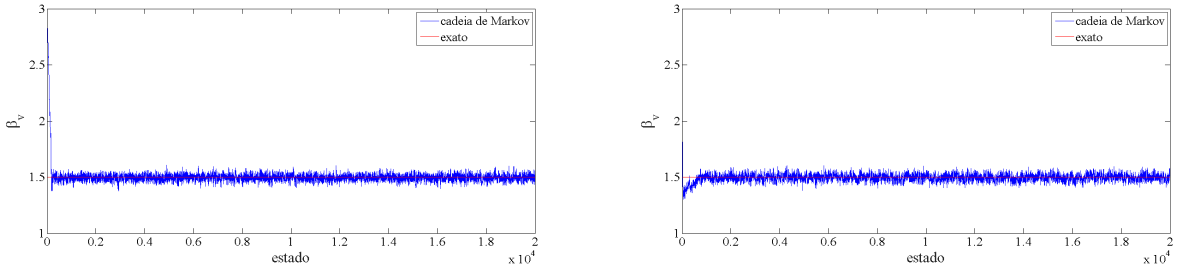

(b) β_v

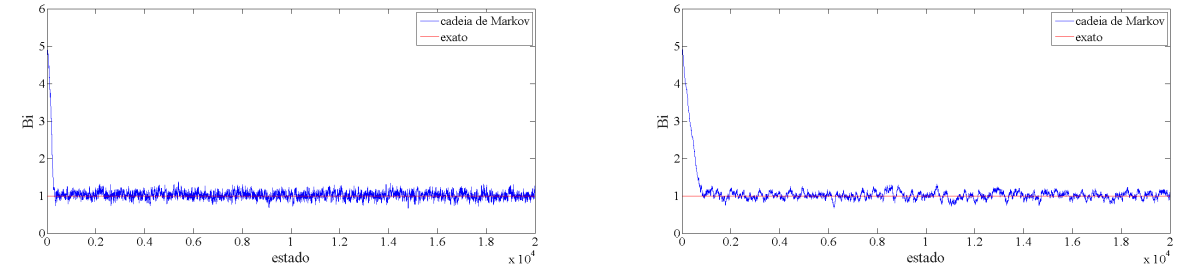

(c) Bi

Figure 3. Markov chain evolution for parameters β_t, β_v and Bi using the Metropolis-Hastings algorithm (left) and the Hamiltonian Monte Carlo method (right).

Table 1. Estimated parameters values with 20,000 states in Markov chains (neglecting first 2,000 states for the chains burning) and the corresponding 95% credibility intervals obtained via MH and HMC for the base case.

Parameter	Exact	Initial	Interval	MCMC	Estimated	Min. with 95%	Max. with 95%
β_v	1.5	3.0	[1, 5]	MH	1.4953	1.4392	1.5513
				HMC	1.4973	1.4400	1.5545
β_t	2.0	3.0	[1, 5]	MH	2.0101	1.6471	2.3730
				HMC	2.0369	1.6270	2.4467
Bi	1.0	5.05	[0.1, 10]	MH	1.0216	0.8340	1.2091
				HMC	1.0114	0.8285	1.1942

Figures 4 (a–c) contains the parameters dispersion via MH (left) and HMC (right). In these figures is possible to visualize the MCMC walks in the parameters space. It is clear to notice a random behavior in the solutions obtained via Metropolis-Hastings algorithm. On the other hand, HMC method presents a faster convergence in the first Markov chains states, heading almost towards to the target solution. However, we notice that both MCMC methods have convergence problems to estimate the β_t parameter, displayed by the high dispersion presented in the parameters space.

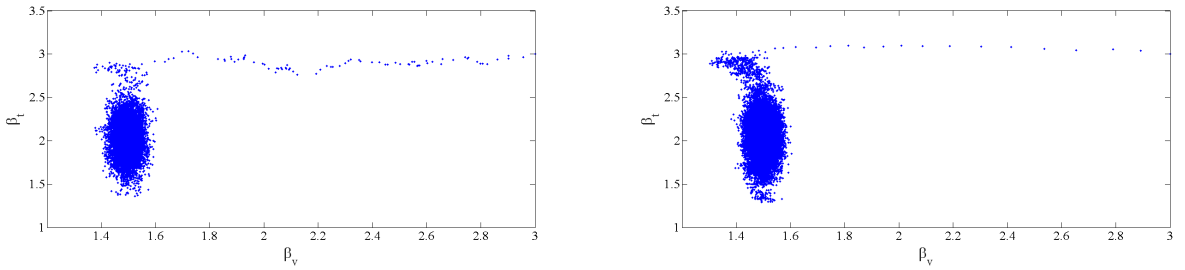

(a) β_v vs. β_t

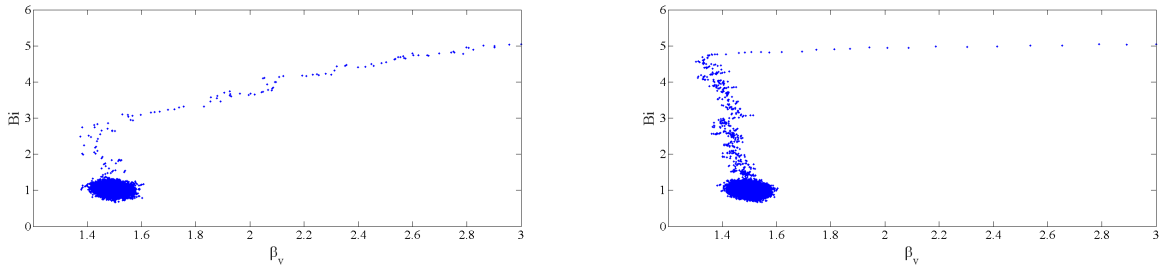

(b) β_v vs. Bi

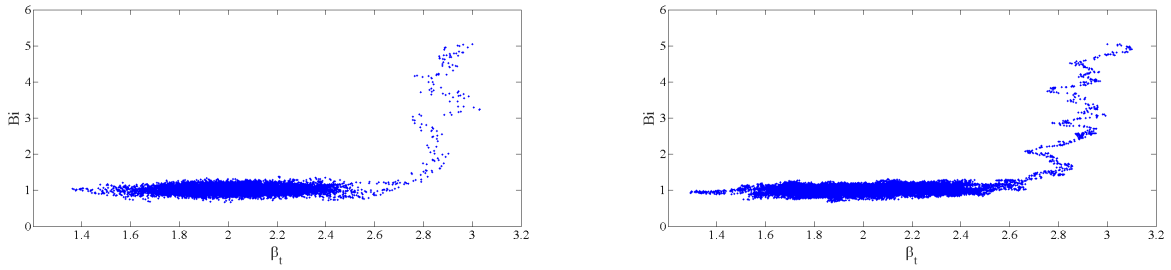

(c) β_t vs. Bi

Figure 4. Parameters dispersion for the base case using the Metropolis-Hastings algorithm (left) and the Hamiltonian Monte Carlo method (right).

Figure 5 (a–c) depicts the autocorrelation of each Markov chain considering one state delay. As for the Markov chains in Figure (2), it can be noticed that the best estimates were achieved for β_v and Bi, whose autocorrelations stayed between the 99% confidence interval for white noise, presenting a more stable solution.

From now on, all the simulations regarding the parameters identification are carried out with just HMC, that proved to be able to achieve Markov chains with improved quality in comparison to the regular MH algorithm.

The next case considered analyzes the effect of different initial guesses for the three parameters. For this purpose, the minimum admissible values were employed for all of them. In Table 2, it can be observed that there is no significant difference in the credibility intervals compared to the base case. This result is expected since the same noise level was used. However, we notice that the estimates were quite worse.

Now, we attempt to illustrate the effect of increasing the standard deviation to 20% of the average values informed as priors for the three parameters, considering the initial guesses employed in the base case. According to Table 3, it seems that these higher standard deviations for the priors affected both the estimates and the credibility intervals, mainly for the β_t parameter.

Finally, we present the last case in which we examine the influence of increasing the uncertainty of the simulated temperature measurements to 10%, while considering the same priors of the base case. In the results presented in Table 4, we see that increasing the noise level from 5 to 10% does not reflect the uncertainty of the measurements in the credibility intervals of the estimates, showing the robustness of the HMC method in the inverse problem solution.

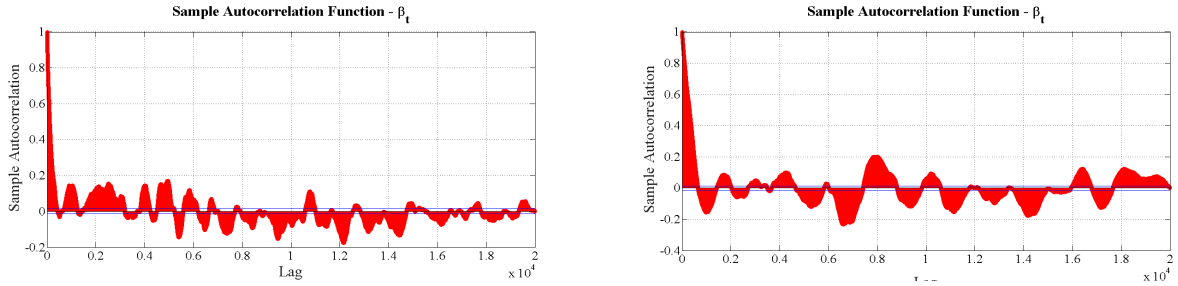

(a) β_t

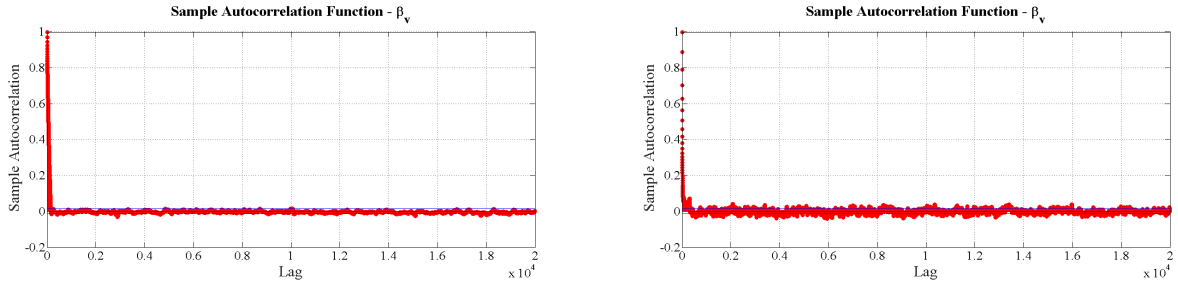

(b) β_v

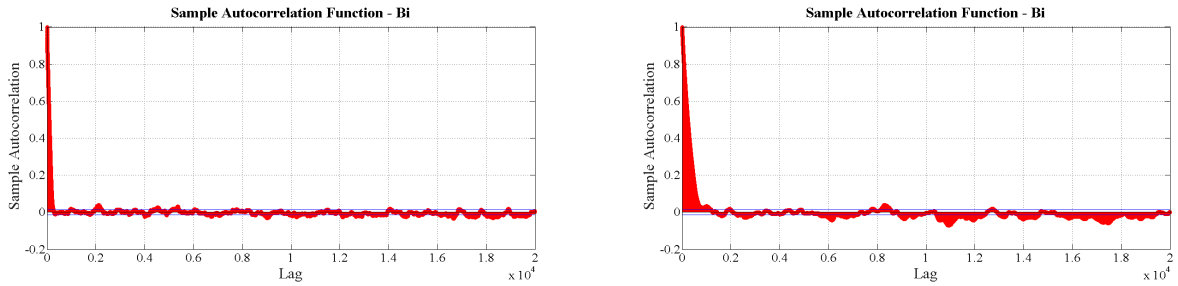

(c) Bi

Figure 5. Markov chains autocorrelations considering one state lag and 99% credibility intervals for white noise using the Metropolis-Hastings algorithm (left) and the Hamiltonian Monte Carlo method (right).

5. CONCLUSIONS

In this work, the inverse analysis of forced convection within micro-channels, focusing on the estimation of the momentum and thermal accommodation coefficients and the Biot number, has been undertaken. It was considered a laminar gas flow within the range of the slip-flow regime. The aim is to demonstrate HMC robustness against random MCMC methods, as Metropolis-Hastings, for the simultaneous estimation of these three parameters, under actual operating conditions of the associated micro-systems.

A simple explicit formulation of finite difference method was implemented in order to solve the direct problem, as well as for obtaining the temperature measurements used in the inverse problem by adding a controlled noise signal.

Due to the low dimensional character of the posterior distribution calculated via the Bayes' theorem, it was not possible to highlight substantial convergence advantages of the HMC front of MH. On the other hand, it was clear to see the deterministic behavior of the HMC convergence in the parameters space. In addition, the solution via HMC provided Markov chains with higher acceptance rates (related to the Hastings ratio, part of the algorithm). In all cases studied, a good agreement between the exact values of the interest parameters and the estimated ones was achieved.

Table 2. Estimated parameters values with 20,000 states in Markov chains (neglecting first 2,000 states for the chains burning) and the corresponding 95% credibility intervals obtained via HMC for different initial guesses (equal to minimum limits).

Parameter	Exact	Initial	Interval	Estimated	Min. with 95%	Max. with 95%
β_v	1.5	1.0	[1, 5]	1.4962	1.4403	1.5520
β_t	2.0	1.0	[1, 5]	1.8911	1.4524	2.3297
Bi	1.0	0.1	[0.1, 10]	1.0224	0.8420	1.2027

Table 3. Estimated parameters values with 20,000 states in Markov chains (neglecting first 2,000 states for the chains burning) and the corresponding 95% credibility intervals obtained via HMC for 20% standard in the priors distributions.

Parameter	Exact	Initial	Interval	Estimated	Min. with 95%	Max. with 95%
β_v	1.5	3.0	[1, 5]	1.4945	1.4349	1.5540
β_t	2.0	3.0	[1, 5]	1.8442	1.2358	2.4525
Bi	1.0	5.05	[0.1, 10]	1.0700	0.7636	1.3763

Table 4. Estimated parameters values with 20,000 states in Markov chains (neglecting first 2,000 states for the chains burning) and the corresponding 95% credibility intervals obtained via HMC for 10% uncertainty in temperature measurements.

Parameter	Exact	Initial	Interval	Estimated	Min. with 95%	Max. with 95%
β_v	1.5	3.0	[1, 5]	1.5038	1.3926	1.6149
β_t	2.0	3.0	[1, 5]	1.9812	1.6583	2.3040
Bi	1.0	5.05	[0.1, 10]	1.0208	0.8200	1.2215

6. ACKNOWLEDGEMENTS

This study was financed in part by the Coordenação de Aperfeiçoamento de Pessoal de Nível Superior - Brasil (CAPES) - Finance Code 001.

The authors also acknowledge the financial support provided by FAPERJ – Fundação Carlos Chagas Filho de Amparo à Pesquisa do Estado do Rio de Janeiro and CNPq – Conselho Nacional de Desenvolvimento Científico e Tecnológico.

7. REFERENCES

Afshar, S. and Sheehan, M., 2018. "Cfd and infrared thermography of particle curtains undergoing convection heat transfer: Image analysis and edge prediction". *Powder Technology*, Vol. 325, pp. 167–179.

Agrawal, A. and Prabhu, S., 2008. "Survey on measurement of tangential momentum accommodation coefficient". *Journal of Vacuum Science & Technology A: Vacuum, Surfaces, and Films*, Vol. 26, No. 4, pp. 634–645.

Ameel, T.A., Wang, X., Barron, R.F. and Warrington, R.O., 1997. "Laminar forced convection in a circular tube with constant heat flux and slip flow". *Microscale Thermophysical Engineering*, Vol. 1, No. 4, pp. 303–320.

Anderson, D., Tannehill, J.C. and Pletcher, R.H., 2016. *Computational fluid mechanics and heat transfer*. CRC Press.

Cotta, R.M., Knupp, D.C. and Naveira-Cotta, C.P., 2016. *Analytical heat and fluid flow in microchannels and microsystems*. Springer.

Hooman, K. and Ejlali, A., 2010. "Effects of viscous heating, fluid property variation, velocity slip, and temperature jump on convection through parallel plate and circular microchannels". *International Communications in Heat and Mass Transfer*, Vol. 37, No. 1, pp. 34–38.

Kaipio, J. and Somersalo, E., 2006. *Statistical and computational inverse problems*, Vol. 160. Springer Science & Business Media.

Kumar, S.R., Reddy, B.K. and Balaji, C., 2017. "Application of hybrid monte carlo algorithm in heat transfer". *Journal of Heat Transfer*, Vol. 139, No. 8, p. 082004.

Larrodé, F.E., Housiadas, C. and Drossinos, Y., 2000. "Slip-flow heat transfer in circular tubes". *International Journal of Heat and Mass Transfer*, Vol. 43, No. 15, pp. 2669–2680.

Metropolis, N., Rosenbluth, A.W., Rosenbluth, M.N., Teller, A.H. and Teller, E., 1953. "Equation of state calculations by fast computing machines". *The journal of chemical physics*, Vol. 21, No. 6, pp. 1087–1092.

Mikhailov, M. and Cotta, R., 2005. "Mixed symbolic–numerical computation of convective heat transfer with slip flow in microchannels". *International communications in heat and mass transfer*, Vol. 32, No. 3-4, pp. 341–348.

Morini, G.L., 2004. "Single-phase convective heat transfer in microchannels: a review of experimental results". *International journal of thermal sciences*, Vol. 43, No. 7, pp. 631–651.

Naveira-Cotta, C.P., Cotta, R.M. and Orlande, H.R., 2010. "Inverse analysis of forced convection in micro-channels with slip flow via integral transforms and bayesian inference". *International Journal of Thermal Sciences*, Vol. 49, No. 6, pp. 879–888.

Neal, R.M. *et al.*, 2011. "Mcmc using hamiltonian dynamics". *Handbook of markov chain monte carlo*, Vol. 2, No. 11, p. 2.

Rader, D.J., Castaneda, J.N., Torczynski, J.R., Grasser, T.W. and Trott, W.M., 2005. "Measurements of thermal accommodation coefficients." Technical report, Sandia National Laboratories.

Rosa, P., Karayiannis, T. and Collins, M., 2009. "Single-phase heat transfer in microchannels: the importance of scaling effects". *Applied Thermal Engineering*, Vol. 29, No. 17-18, pp. 3447–3468.

Rostami, A., Mujumdar, A. and Saniei, N., 2002. "Flow and heat transfer for gas flowing in microchannels: a review". *Heat and Mass transfer*, Vol. 38, No. 4-5, pp. 359–367.

Torres, M.P., Silva, G.R., Stutz, L.T., Knupp, D.C. and Neto, A.J.S., 2018. "Application of the hamiltonian monte carlo method for thermal properties estimation in thin plates". In *III Simposio Internacional de Modelación aplicada a la Ingeniería*.

Yu, S. and Ameel, T.A., 2001. "Slip-flow heat transfer in rectangular microchannels". *International Journal of Heat and Mass Transfer*, Vol. 44, No. 22, pp. 4225–4234.

8. RESPONSIBILITY NOTICE

The authors are the only responsible for the printed material included in this paper.